

CARBO - The Carbon Observatory Instrument Suite – the next generation of Earth observing instruments for global monitoring of carbon gases

J. Kent Wallace*^a, Charles Miller^a, Shannon Kian Zareh^a, Amy Mainzer^a, Thomas S. Pagano^a,
Cynthia B. Brooks^b, Daniel T. Jaffe^b, Dan Wilson^a, Annmarie Eldering^a, Dejian Fu^a,
Randall Bartos^a, Yuri Beregovski^a, Mayer Rud^a, James P. McGuire^a,
Andre Wong^a, Didier Keymeulen^a, Peter Sullivan^a, Elliott Liggett^a, Michael Bernas^a
^aJet Propulsion Laboratory/California Institute of Technology, 4800 Oak Grove Dr., Pasadena, CA,
USA 91106-8099;

^dDepartment of Astronomy and McDonald Observatory, The University of Texas at Austin, 2515
Speedway, Austin, TX 78712

ABSTRACT

The Carbon Observatory Instrument Suite, or CARBO, consists of four carbon observing instruments sharing a common instrument bus, yet targeted for a particular wavelength band each with a unique science observation. They are: a) Instrument 1, wavelength centered at 756 nm for oxygen and solar-induced chlorophyll fluorescence (SIF) observations, b) Instrument 2, centered at 1629 nm, for carbon dioxide (CO₂) and methane (CH₄) observation, c) Instrument 3, centered at 2062 nm for carbon dioxide and d) Instrument 4, centered at 2328 for carbon monoxide (CO) and methane. From low-Earth orbit, these instruments have a field-of-view of 10 to 15 degrees, and a spatial resolution of 2 km square. These instruments have a spectral resolving power ranging from ten to twenty thousand, and can monitor column-average dry air mole fraction of carbon dioxide (XCO₂) at 1.5 ppm, and methane (XCH₄) at 7 ppb. These new instruments will advance the use of immersion grating technology in spectrometer instruments in order to reduce the size of the instrument, while improving performance. These compact, capable instruments are envisioned to be compatible with small satellites, yet modular to be configured to address the particular science questions at hand.

Here we report on the current status of the instrument design and fabrication, focusing primarily on Instruments 1 and 2. We will describe the key science and engineering requirements and the instrument performance error budget. We will discuss the optical design with particular emphasis on the immersion grating, and the advantages this new technology affords compared to previous instruments. We will also discuss the status of the focal plane array and the detector electronics and housing. Finally, we report on a new approach – developed during this instrument design process - which enables simultaneous measurement of both orthogonal polarization states (S and P) over the field-of-view and optical bandpass. We believe this polarization sensing capability will enable science observations which were previously limited by instrumental and observational degeneracies. In particular: improved sensitivity to all species, better sensitivity to surface polarization effects, better constraints on aerosol scattering parameters, and superior discrimination of the vertical distribution of gases and aerosols.

Keywords: satellite remote sensing, Carbon Dioxide (CO₂), Methane (CH₄), Carbon Monoxide (CO), earth-observing

1. INTRODUCTION

Monitoring carbon gases in the atmosphere is increasingly important as we try to understand our changing climate [1]. Many instruments have been built and flown or proposed to monitor these gases from space [2,3,4,5,6], and there are results from several of these instruments [2,3,4,5]. Here we introduce a new observing mode and architecture for an instrument suite we call CARBO (The Carbon Balance Observatory). This instrument advances the field in the following ways: 1) it is a wide-field instrument initially conceived to have a field-of-view (FOV) of 10 to 15 degrees, 2) it uses immersion gratings for the dispersion element 3) it will sense both polarization states independently and simultaneously, and 4) it takes full advantage of the imaging arrays for Earth observing.

*james.k.wallace@jpl.nasa.gov; phone 1 818 393-7066; www.jpl.nasa.gov

1.1 CARBO Overview

CARBO [7] is funded by the Earth Science Technology Office (ESTO) by their Instrument Incubator Program (IIP). This program funds projects to develop new technologies to infuse them into future instruments. The key technology driver for this program is immersion gratings. The benefit of immersion gratings is that dispersion occurs ‘inside’ the grating material where the wavelength is scaled down by the index of refraction. This gain can be significant, particularly when the optical index of refraction is large, such as for silicon. (We will discuss this and other benefits of immersion gratings in greater detail later.)

Our goal is to design, build and deploy two instruments that will use immersion gratings as the dispersing element. We will also design and analyze two more instruments that will be for the near infrared. These instruments are designed to be compatible with future, space flight observatories. However, they will initially be deployed and tested on either ground-based and/or airborne platforms.

1.2 CARBO Science

Table 1 below summarizes the capabilities of the four CARBO instruments. Monitoring the atmospheric abundance of carbon diode, carbon monoxide and methane is the key requirement. Instrument 1 also monitors the oxygen A line, as well as the solar induced chlorophyll fluorescence (SIF). Instrument 2 will measure carbon dioxide and methane. Instrument 3 will measure carbon dioxide. Instrument 4 will measure carbon monoxide and methane.

The spatial resolution of the instrument is 2 km x 2 km. This spatial resolution is selected in order to maximize the likelihood of cloud-free observations.

	Wavelength Range	Wavelength resolution ($\delta\lambda$)	Spectral Pixels, Nyquist ($2 \Delta\lambda/\delta\lambda$)	Spectral Resolving Power ($\lambda/\delta\lambda$)	Science	Required SNR
Inst. 1	745 – 772 nm $\bar{\lambda} = 758.5, \Delta\lambda = 27$ nm	0.05 nm	1080	15,400	O ₂ , SIF	>300
Inst. 2	1598-1659 nm $\bar{\lambda} = 1628.5, \Delta\lambda = 61$ nm	0.15 nm	814	11,060	CO ₂ , CH ₄	>350
Inst. 3	2045 – 2080 nm $\bar{\lambda} = 2062.5, \Delta\lambda = 35$ nm	0.1 nm	700	20,800	CO ₂	>150
Inst. 4	2305 – 2350 nm $\bar{\lambda} = 2327.5, \Delta\lambda = 45$ nm	0.12 nm	750	19,583	CO, CH ₄ , H ₂ O _b	>100

Table 1. The performance of the four CARBO instruments is summarized in the table above which describes the spectral properties, the resolving power and science observable. The required SNR ties the science extraction to the required instrument performance. We will build Instruments 1 and 2 as part of this activity, while Instruments 3 and 4 will be designed.

Figure 1, below, shows the spectrum of the light (0 degree solar zenith angle, 100% albedo) after a double pass through the Earth’s atmosphere for the four spectral bands covered by the CARBO instrument suite. These spectra are sampled at twice the required spectral resolution of the instrument and clearly show the strong absorption features used to extract the atmospheric abundance. The radiant flux from this model are used as inputs to the instrument performance model which will be discussed later.

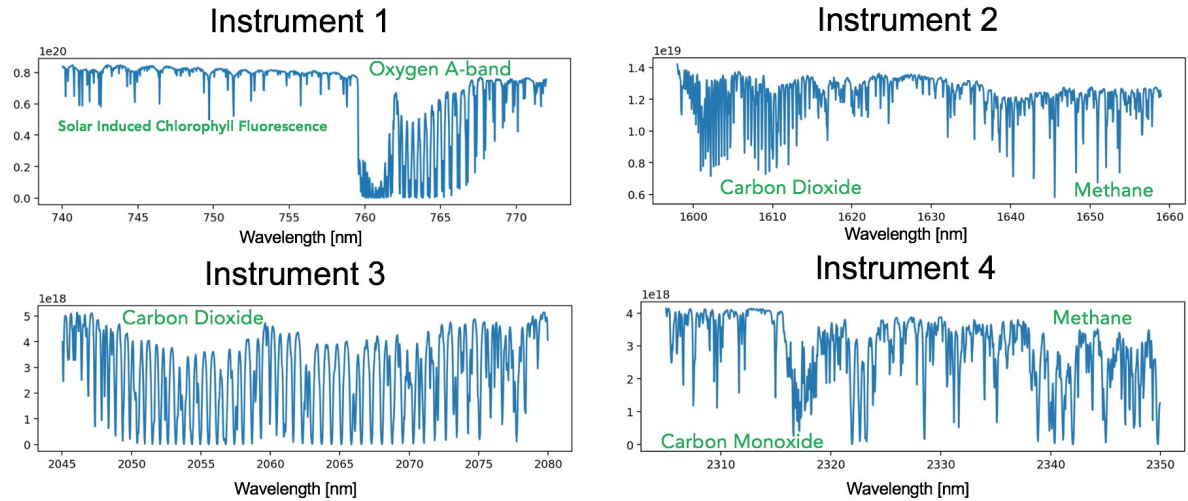


Figure 1. The spectral range of the four CARBO instruments allow measurements of many atmospheric constituents. Instrument 1 measures Solar Induced Chlorophyll Fluorescence and the Oxygen A band. Instrument 2 measures Carbon Monoxide and Methane. Instrument 3 measures Carbon Monoxide, and Instrument 4 Carbon Monoxide and Methane.

1.3 Observational Orbit

The CARBO instruments are designed to be operated in low-earth orbit (LEO). We assume a nominal altitude of 705 kilometers. At this altitude, the orbit period is 98.73 minutes, and the orbit ground velocity is 6.767 km/sec. At this orbit ground velocity, one kilometer is covered in 147.8 milliseconds (6.767 Hz). We note that sampling of a 1 km spatial scale along the track of the satellite orbit requires a temporal sampling rate of 6.8 Hz. Although this sampling rate seems rather slow given the abundance of solar photons reflected from the Earth, the relatively high spectral dispersion results in counts per pixel that are quite modest, and noise properties of the detectors are significant contributors to the system performance.

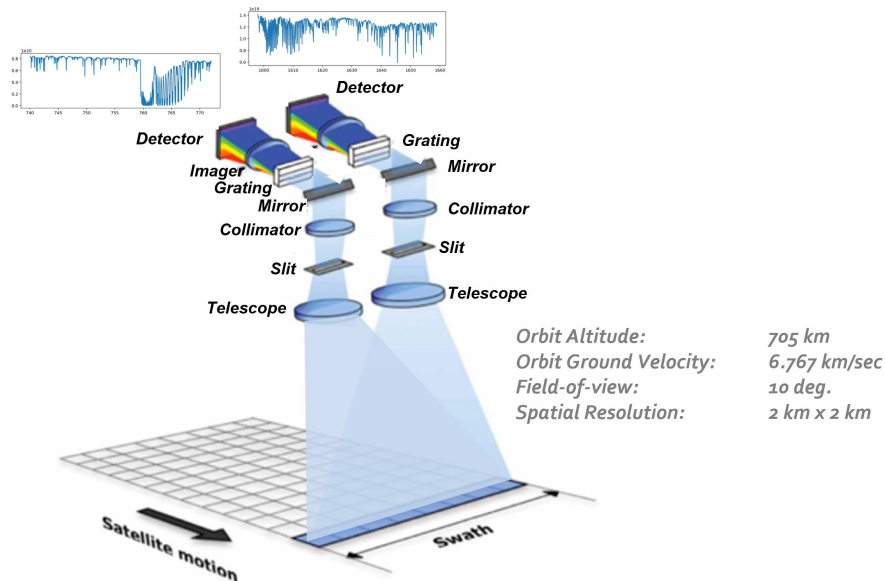


Figure 2. The schematic diagram of the orbit for two of the four CARBO instruments is shown above. At the low-earth orbit altitude of 705 km, the orbit ground distance is 6.767 km/sec. At this speed, a 1-kilometer long path along the track of the satellite motion takes 147.8 milliseconds of time. The individual CARBO instruments are independent, yet share the same mechanical instrument carrier. They are co-aligned in order to view the same ground scene simultaneously. The instruments cover different spectral bands for different observations.

2. KEY TECHNOLOGY COMPONENTS

One goal of NASA’s Earth Science Technology Office’s Instrument Incubator Program is to infuse new technologies into future missions. One key technology for this particular program is the immersion grating. This technology holds the promise of reducing the size of spectrometer instruments which would otherwise use echelle gratings. This promise is indeed bearing out, but there are other benefits to this technology too. However, we are also pursuing two more other new technologies that are also being developed with CARBO program.

Detectors continue to drive the performance of a system, and therefore continue to have strong leverage over system complexity and performance. Our baseline instruments will be the CHROMA-A detector from Teledyne, Inc., and these detectors have a distinct advantage in terms of operations over more traditional imaging arrays. However, we are also implementing the CHROMA-D detector which has significant advantages due in part to the great reduction in electronics and the image chain simplification with a direct, digital output.

Finally, we are implementing an instrument architecture whereby both polarizations are sensed simultaneously. This new capability is implemented with the addition of a couple of polarization components, but otherwise is unobtrusive to the instrument. Our polarization sensing approach has other unexpected benefits as well. The engineering trade for this polarization sensing capability is that our current array size defines the FOV.

2.1 Immersion Grating

For instruments with moderate to high spectral resolving power, the dispersion element of choice is the echelle grating. The shape of the surface of the grating has the appearance of a micro staircase – with a pitch ($\Lambda = 1/\text{period}$), and blaze angle, θ_B . Light, upon reflection from the grating, will constructively interfere when the pathlength difference between adjacent grating facets are equal to an integer number of wavelengths according to the grating equation:

$$\sin[\theta_i] - \sin[\theta_r] = m \lambda / (n[\lambda] \Lambda) \quad (1)$$

Here, the incidence and reflected angles are θ_i and θ_r respectively, the diffraction order is given by the integer m , the wavelength is given by λ , and the index of refraction is $n[\lambda]$. For echelle gratings used in air, the index of refraction is unity. However, for immersion gratings, the light enters the substrate first, and then undergoes the effect of the echelle. Inside the glass, the wavelength is scaled by the index of refraction: $\lambda' = \lambda/n[\lambda]$. To maintain the same spectral resolving power, the grating period, and thus the whole grating, can also be reduced by the index of refraction. For instruments in the near infrared (our Instrument 2, for instance), where silicon can be used, this results in a significant reduction in size because the index of refraction, 3.47, is quite large.

Our collaborators at the University of Texas – Austin, Cinthia Brooks and Dan Jaffee, have been fabricating silicon immersion gratings for astronomical instruments for more almost two decades. Their instruments include: IGRINS, iSHELL with plans for GMTNIRS [8,9,10,11,12,13]. Fabrication with silicon offers the advantage of anisotropic chemical etching along crystalline planes. This process results in the grating structures that are accurate and smooth at the atomic level. For our instrument, we prefer to work at low diffraction orders. The result is feature sizes on the immersion grating that are reaching small spatial scales never seen before. Our technology development therefore continues to push this technology forward into new areas. Figure 3 below illustrates the fabrication capabilities of this team.

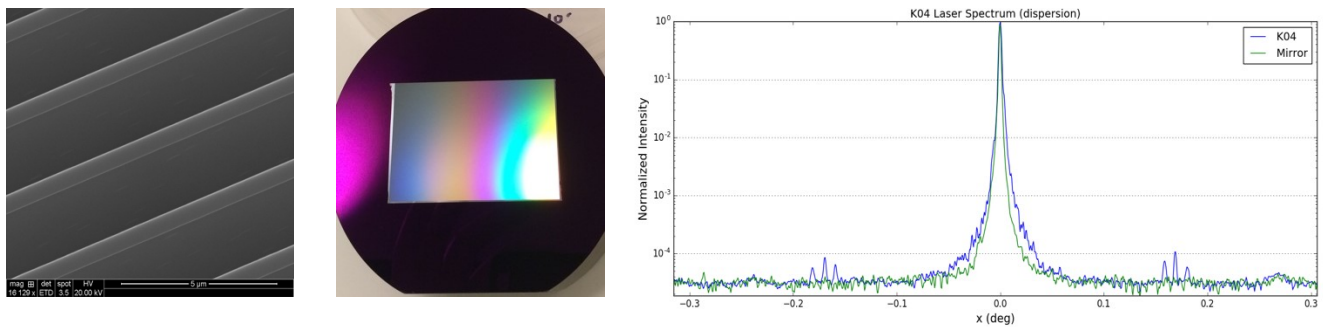


Figure 3. Images of the groove structure, completed prototype grating and stray light characteristics of a Si immersion grating fabricated to CARBO characteristics under the UT/JPL ACT project [8].

There are other benefits to the use of immersion gratings worth nothing. A typical grating will, upon reflection, distort the incoming beam by different amounts in the two orthogonal directions. For instance, an incident circular beam is transformed into an elliptical, egg-shaped beam upon reflection – this un-diffracted direction is unchanged, while the diffracted direction is compressed. This is known as anamorphic beam compression, and results in an asymmetric point-spread function (PSF) in the final image plane. However, this anamorphic remapping of the pupil can be largely compensated by the action of a compensating prism – either integral to the immersion grating itself or a separate element used in conjugation with the immersion grating such that the total power of the prism elements compensates the intrinsic anamorphic imaging of the grating. This is shown below in Figure 4. The result of anamorphic correction is that the spectral resolving power is much more uniform, because the PSF is more uniformly symmetric over wavelength and therefore properly sampled by the detector in a more uniform way. Specifically, with a traditional air grating the spectral resolving power varies by a factor of 1.8 over the band. With compensation, however, this can be reduced to a variation of 1.08 – an order of magnitude improvement. This is shown below in Figure 5.

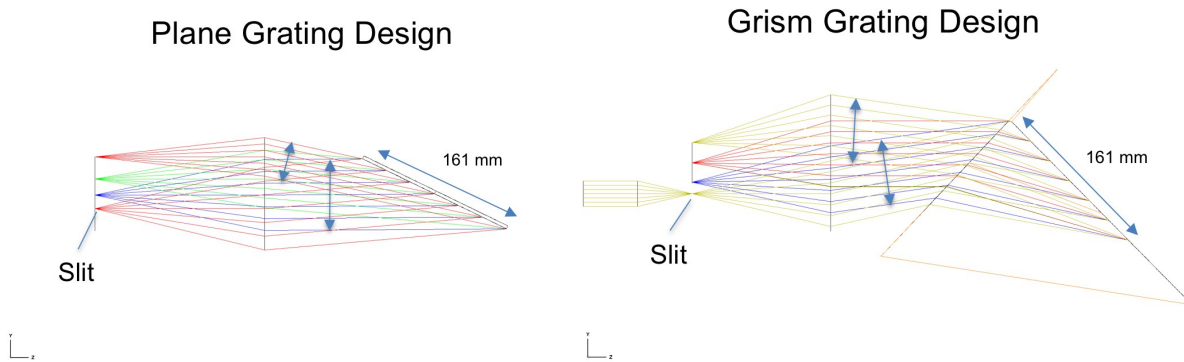


Figure 4. Anamorphic beam compression is very different between the traditional, plane grating design on the left, and the compensated immersion grating design on the right. Upon reflection from both gratings, the input pupil is distorted in the vertical direction as illustrated by the in-plane beam sizes on the left-hand image. However, by taking advantage of the compensating effect offered by the prism, the difference in pupil size can be reduced by an order of magnitude.



Figure 5. The benefit of correcting the anamorphic imaging with the compensating prism of the immersion grating, is to make the spectral resolving power of the instrument more uniform. The variation in spectral resolving power for the air grating varies by a factor of 1.8, whereas the variation for the immersion grating with prism compensation is 1.08 – an order of magnitude reduction.

2.2 Detectors

Our baseline detectors are the CHROMA-A from Teledyne. They are a new generation of detectors specifically for Earth-observing applications. They have a generous well depth ranging from 600K to 1M electrons. The array size of

480 pixels by 1280 pixels is compatible with our baseline image plane footprint. (From Table 1, we require 1080 pixels in the spectral direction for Nyquist sampling.) The pixel size is 30 μm x 30 μm resulting in a physical size of the array of 14.4 mm by 38.4 mm. The specific detectors available for our instrument have a cutoff wavelength of 2.5 μm , so we require a cold filter to limit the thermal background from the warm optics. JPL has a long history of using these detectors for spectrometer instruments. Our performance budget is driven by the measured noise of the detectors – dark current, quantization noise, and read noise.

The CHROMA–A detectors require a suite of support electronics: analog readout, detector power, and analog-to-digital conversion. The fabrication of two sets of electronics are nearing completion for our two baseline instruments, and we expect to have a full signal chain from the two sets of electronics well in advance of the calendar year end.

However, we are also securing a CHROMA-D detector. This detector has 512 pixels x 2048 pixels, with a pixel size of 18 μm resulting in an array size of 9.216 mm by 36.864 mm. This array is slightly smaller than the CHROMA-A detector, and thus can replace the CHROMA-A with only modest loss of spatial coverage. The benefit of the CHROMA-D is the digital output from the array. This greatly reduces the complexity of the signal chain electronics, while also preparing our instrument development to be more directly applicable for future flight instruments. CHROMA-D electronics generate more heat at the location of the focal plane array, so thermal management must be different between the two devices, but this is not a fundamental issue with regards to operation.

2.3 Polarization Sensing

All gratings, both air and immersed, respond to the two orthogonal polarization states in different ways – sometimes radically different. This difference in response is captured most accurately in the grating efficiency versus wavelength for the two different polarization states. This difference in polarization state is most pronounced when the grating period is on the order of the wavelength of light. Therefore, for gratings working at first order ($m=1$, Eq. 1), the wavelength inside the material is 495.8 nm, and the grating period is 292.4 nm which is much smaller than the wavelength. By creating a grating that works at higher order, like $m=4$, the period increases by $4 \times 292.4 \text{ nm} = 1,169.4 \text{ nm}$ which is now greater than the immersion wavelength by about a factor of two, and the grating efficiency is much less polarization sensitive. This is shown below in Figure 6.

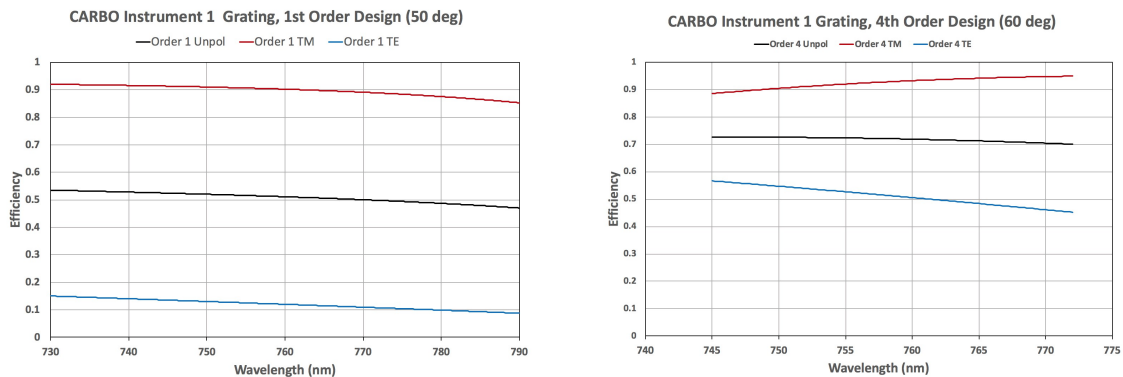


Figure 6. Echelle gratings of all types are polarization sensitive. The plot on the left illustrates the polarization sensitivity for an immersion grating working at first order, where the grating period (292.4 nm) is smaller than the immersion wavelength (495.8 nm). By designing a diffraction grating to work at higher order (here, $m=4$), the polarization sensitivity can be reduced, but not entirely eliminated. Working at a higher diffraction order also makes the fabrication of the grating more challenging because of greater susceptibility to fabrication errors.

However, the difference in grating efficiency is still quite large, even at the higher order. For instance, for the right-hand plot of Fig. 6, the difference in efficiency between the two polarization states at the long wavelength is $\sim 50\%$.

This is problematic for science observations because atmospheric constituents such as aerosols also act as polarizing elements. This causes a degeneracy between the polarization effects of the atmosphere and the polarization state of the instrument. The traditional solution to this degeneracy is to add a linear polarizer to the instrument in order to firmly establish its polarization state, but this is at the cost of half of the light – thereby reducing the detection signal-to-noise ratio. (SNR).

Our solution to this polarization problem is to sense both polarization states simultaneously. This is done by the addition of two polarization components: 1) a traditional Wollaston prism at the telescope input, and 2) a polarization rotation element at the focal plane. These two elements work in the following way, the Wollaston splits the two different polarization states angularly with one polarization state getting an additional tilt angle up, and the orthogonal polarization getting a tilt angle down. After the telescope imaging system, in the slit focal plane, the two polarization states are spatially separated. The second, custom polarization element is in the focal plane. On one half of the image plane we use a true zero-order half-wave plate, oriented at 45 degrees to rotate this polarization state into the other, orthogonal polarization state. On the other half of the focal plane is also a true zero-order half-wave plate, but oriented at 0 degrees. This has no effect on the polarization state, but exactly matches the pathlength of the first side of the image plane. The light then passes through the slit. At this point, the two beams: 1) have been spatially encoded before the slit to reflect the orthogonal polarization states coming into the system, but 2) now have the identical polarization state internal to the instrument. On the opposite side of the slit is a linear polarizer which is aligned to the single polarization state of both beams. This architecture is shown below in Figure 7.

This polarization state internal to the spectrometer is aligned to the grating to give us maximum diffraction efficiency. In this way, the grating efficiencies for both polarization states are maximum and they are identical. With reference to Fig. 5, this means that internal to the instrument, blue curve moves up and becomes identical to the red curve. This method also allows us to fabricate the grating at the lowest diffraction order which: 1) increases the diffraction efficiency and 2) relaxes fabrication tolerances. By relaxing the fabrication tolerances, we are able to expand the possible sources for the immersion grating (both vendors and methods).

There are additional benefits to sensing both states simultaneously. First, we are using all the available light to make our measurements – no polarizer is being added to system which would remove half the available photons. Second, simultaneous polarization sensing allows us to extract additional science measurements with are otherwise unavailable, namely: 1) improve the modeling degrees of freedom for all species, 2) enhance the sensitivity to the surface bi-direction reflectance distribution function (BRDF) including polarization effects 3) improve the sensitivity to aerosol composition (providing better constraints on scattering parameters) and better discrimination of atmospheric and surface scattering and 4) enable superior discrimination of the vertical distribution of CO₂, CH₄, CO and aerosol profiles.

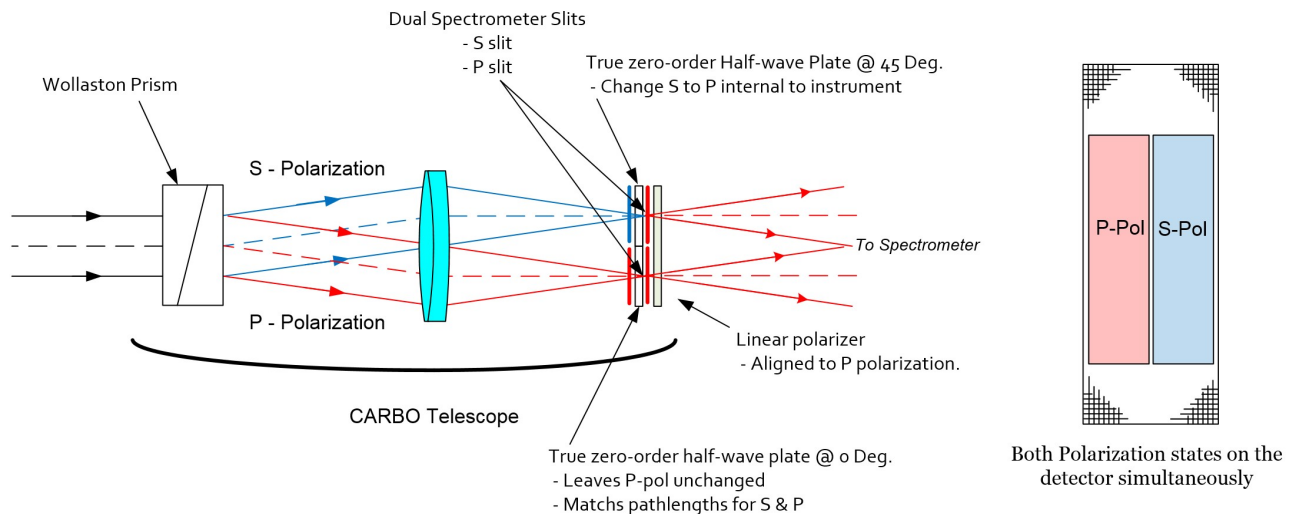


Figure 7. Simultaneous dual-polarization sensing can be implemented using the architecture illustrated here. There are two optical elements that are added to the nominal system: 1) the Wollaston Prism to angularly differentiate the polarization states at the input to the telescope, and 2) the custom polarization rotation element. The two orthogonal input polarization states are spatially encoded at the slit, but then rotated to be identical internal to the spectrometer instrument itself. In this way, the grating: 1) is used at the lowest diffraction order, 2) works at the highest grating efficiency, and 3) perfectly matches the grating efficiencies of both polarizations.

In order to implement this dual-polarization sensing, we needed to trade detector pixels between field-of-view on the ground versus pixels used for polarization sensing. As such, we have reduced our field of view to 7.5 degrees for Instrument 1 and 5 degrees for Instrument 2. However, larger format detectors will allow us to increase our field of view to the nominal 15 degrees. Our investment in CHROMA-D detector development has direct and immediate payoff as we

consider larger detector formats. Although our baseline CHROMA-D is 512 pixels by 2048 pixels, these arrays are available in 1536 pixels x 2048 pixels, which is compatible with our spectral sensing requirements, and returns us to our original 7.5 deg FOV requirements without impacting the dual-polarization sensing architecture.

3. BASELINE INSTRUMENT DESIGNS

In this section, we synthesize the key aspects presented into preliminary optical designs for Instruments 1 and 2. The guiding tool for this performance error budget which considers: the radiometry over the band, the observational scenario, the instrumental parameters, the throughput of the system, the noise performance of the detector, and the integration time. By adjusting these parameters, we can establish the first order properties of the system which meet our system SNR requirement. These first order properties, along with other fabrication constraints, are used as a starting point for the optical design. With this preliminary optical design, we show the conceptual opto/mechanical design for each instrument with particular detail to the detector housing and the optical feed for the Littrow layout.

3.1 Spectrometer Performance Modeling

Lacking a detailed, end-to-end performance model of the system, our team uses an equally powerful, yet simple way of guiding the engineering design work via an analysis of the SNR per instrument. As flux inputs, we consider the radiometry, double pass through the Earth's atmosphere. This is provided by our science team at a spectral resolution of twice the required wavelength resolution per instrument. We then scale this by the albedo (here, 5%), and the solar zenith angle (65 Degrees). The area-solid angle product, $A\Omega$, is the area of the lens multiplied by the area imaged on the ground, divided by the square of the satellite altitude. We chose to Nyquist sample the short width of the slit by two, 30-micron detector pixels, and our spectrometer relay from the slit to the detector is nominally 1:1. It is this 60-um slit, imaged on the ground by the telescope that defines the ground area. The satellite motion and detector integration time are used to establish the 1km sample distance along the trajectory on the ground. Per our previous discussion, this is 147.8 milliseconds. Two of these integrations are the Nyquist sampling on the ground in the direction of the satellite motion. We are free to choose the focal length of the telescope to sample along the transverse spatial dimension. The constraints are simply that we must have enough pixels on the array to sample the field-of-view, (more pixels corresponds to a slower $f/\#$) and that we don't sample too many pixels thereby reducing the SNR (less pixels means faster $f/\#$).

The detector properties for the CHROMA-A are a key to the performance of the instrument. This is somewhat counter-intuitive given the bright solar illumination and the large solid angle. However, our spectrometers have high spectral resolution, and the bandpass per spectral channel is quite small (50 and 150 *picometers*, for Instruments 1 and 2, respectively). For the CHROMA-A we assume the following detector properties: Dark Current: 1000 e's per second, read noise: 80 e-, rms, quantization noise: 10.7 e- per pixel, electronics noise: 70 e-, rms.

Using these inputs, we have the following first-order design starting points: Instrument 1: Telescope aperture diameter: 25 mm, Telescope focal length: 52.8 mm, Telescope $f/\#$: 2.11, Ground Sample Distance: 400 m (5 pixels per 2 km). Likewise, the first order properties for Instrument 2 are: Telescope aperture diameter: 39.78 mm, Telescope Focal length: 76.14, Telescope $f/\#$: 1.92 and Ground Sample Distance: 278 m (~ 7 pixels per 2 km).

3.2 Instrument 1 Preliminary Design

The optical layout of the Instrument 1 is given below in Figure 8. Light enters from the top of the image, and the first element in the system, a rectangular object, is the Wollaston prism. This applies an angular separation between the two orthogonal polarization states. The next optical assembly, the telescope, immediately follows. It consists of four optical elements which form an image at the slit matching the $f/\#$ derived from the performance modeling. At the focal plane is the split polarization element, which rotates half of the field that is in one state, into the orthogonal polarization state while leaving the other half of the focal plane unchanged. After these two beams pass through the slit, a linear polarizer after the slit prevents leaking of off-axis and orthogonal polarization states to pass through. A fold mirror directs the incoming light through the first pass of the Littrow optics, through the prism to the immersion grating. On the return, the rays make a second pass through the Littrow optics, passing just below the fold mirror, through the detector window, through a cold filter and onto the detector.

The size of the Littrow optics and the immersion grating are quite large. Therefore, we have carefully selected materials that are available in large sizes, and with very low inhomogeneities. We have performed design studies to quantify the

benefit (if any) of using aspheric elements. The system below has two aspheric surfaces, and reduces the number of elements in the system from six to four (shown here).

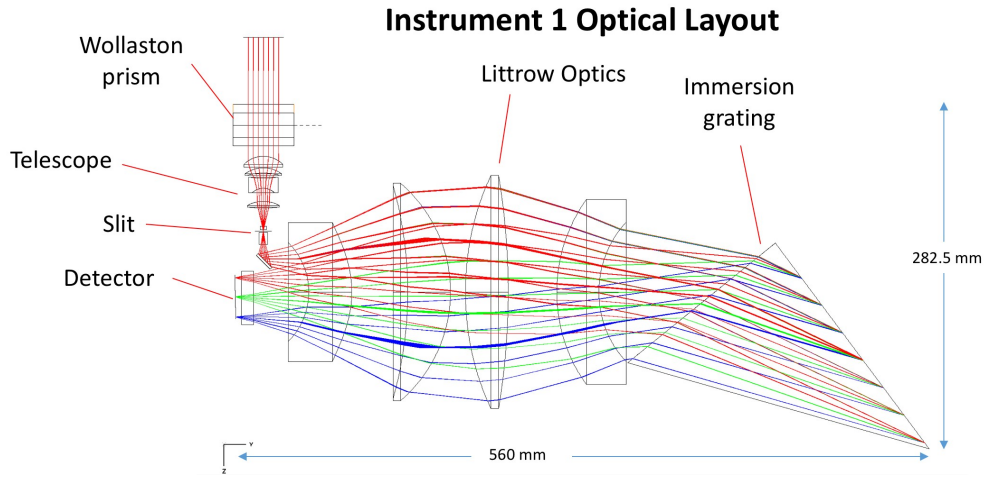


Figure 8. This image shows the preliminary optical design for CARBO Instrument 1. Light enters from the top through the Wollaston prism and Telescope, passes through the slit, and is folded towards the right passing through the Littrow optics to the prism/immersion grating. The return trip passes again through the Littrow optics through a camera housing window to the detector.

The input optics are illustrated in detail below in Figure 9. These rays only trace the system up to the focal plane slit. They will be specified and procured as part of a stand-alone assembly that will be attached to the other key elements of the optical system: the Littrow optics, the immersion grating, and the camera housing. These elements are all spherical and use readily available materials with glasses that are frequently melted.

Instrument 1 Front Optics: Wollaston and Telescope

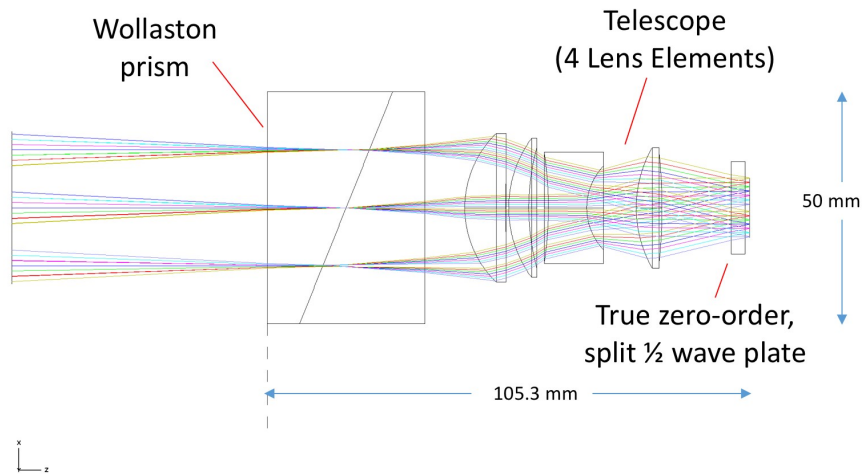


Figure 9. A detail of the CARBO Instrument 1 front optics is illustrated above. Light enters the system from the left, the orthogonal polarizations are split at the Wollaston prism before entering the telescope optics. Immediately before the slit, the focal plane is spatially split into the two orthogonal polarization states, but the custom, true zero-order half-wave plate rotates the two polarizations to be identical internal to the spectrometer instrument.

3.3 Instrument 2 Preliminary Design

The optics for CARBO Instrument 2 are illustrated below in Figure 10, and follow an almost identical path as Instrument 1: polarization separation, input telescope, polarization rotation at the focal plane slit, Littrow optics, immersion grating, and detector optics. However, a major difference is the implementation of the silicon immersion grating. The immersion

grating/prism assembly was divided into two separate elements due to constraints on the element size imposed by the fabrication method. The silicon immersion grating is a led by our collaborators at the University of Texas – Austin.

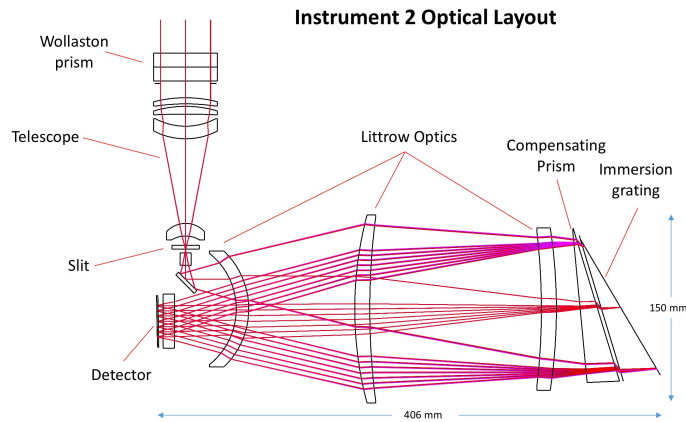


Figure 10. The preliminary optical design for Instrument 2 is shown in the diagram above. Light enters from the top, passes through the Wollaston prism, then then through the telescope to the slit in the image plane. A fold mirror directs the beam to the right, through the Littrow optics, to the compensating prism/immersion grating pair. (These two elements are separate due to fabrication limitations for the silicon etching.) On the return path, the light one again passes through the Littrow optics through the camera housing window to the detector plane.

The fore optics to Instrument 2 are highlighted below. These optics have the identical functionality of Instrument 1, and therefore look nearly identical – with only slight differences in aperture size. The polarization split is the first component, imaging optics (four lenses, all spherical) produce an image at the slit where the polarization split element is located.

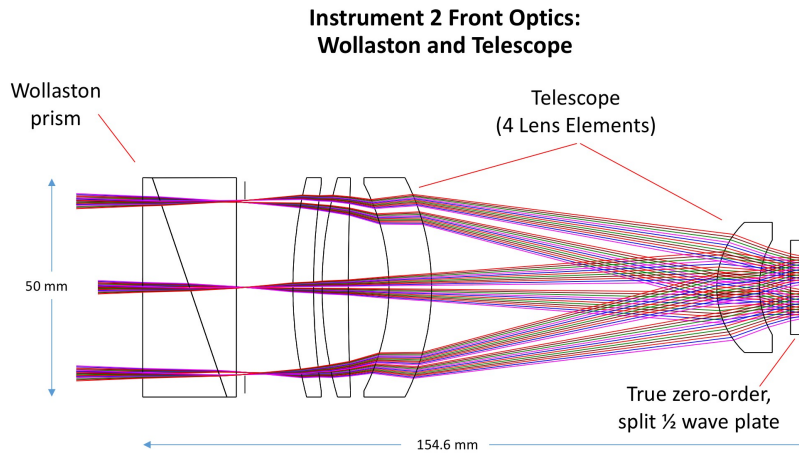


Figure 11. The front optics of CARBO Instrument 2 are shown above. Light enters from the left, passes through the Wollaston prism which angularly separates the two orthogonal polarization states. The telescope optics form an image of the two polarization states in the slit plane. A custom, split true zero-order half-wave plate rotates the polarization in one half of the field into the other polarization state. After the slit, the polarization state from both halves of the image plane are identical from the perspective of the spectrometer instrument. This polarization splitting and simultaneous sensing increases the throughput of the system, and enables new science observations.

3.4 Conceptual Instrument Mechanical Design

We have generated a conceptual opto/mechanical design for both Instruments 1 and 2. Our general approach is to compose the system of four main components: 1) the input telescope, 2) the Littrow optics 3) the immersion grating, and 4) the camera housing. We note that for these first two instruments, only detector needs to be cooled (due to it’s long cutoff wavelength). The telescope optics, and Littrow optics will be stand-alone assemblies. The camera housing will

also be designed and fabricated as its own element. The immersion grating opto/mech design work will be done in-house given that the optical elements themselves are fabricated in close collaboration with JPL.

Instrument 1: Conceptual Mechanical Layout

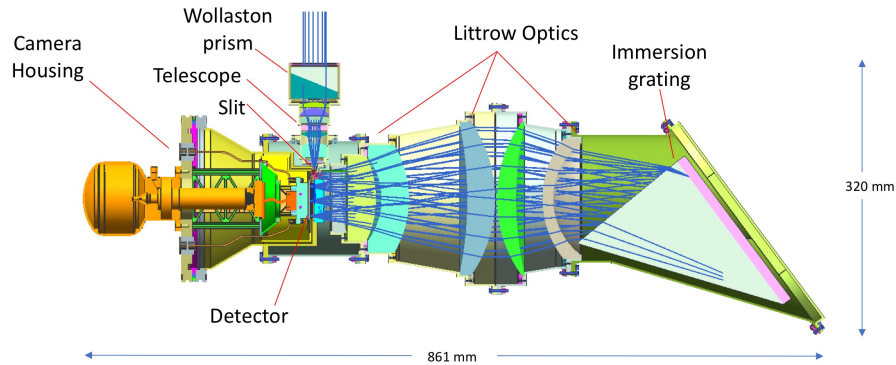


Figure 12. Simultaneous dual-polarization sensing can be implemented using the architecture illustrated here. There are two optical elements that are added to the nominal system: 1) the Wollaston Prism to angularly differentiate the polarization states at the input to the telescope, and 2) the custom polarization rotation element. The two orthogonal input polarization states are spatially encoded at the slit, but then rotated to be identical internal to the spectrometer instrument itself. In this way, the grating: 1) is used at the lowest diffraction order, 2) works at the highest grating efficiency, and 3) perfectly matches the grating efficiencies of both polarizations

The opto/mech for Instrument 2 is shown below in Figure 13. This instrument shares the same four core components as Instrument 1. The camera housing is also designed to be completely compatible between the two instruments with identical interfaces. This commonality in instrument detector housing and cooling will make operations and maintenance easier. Both instruments share a similar mechanical envelope, which will make co-mounting both on a common instrument platform feasible.

Instrument 2: Conceptual Mechanical Layout

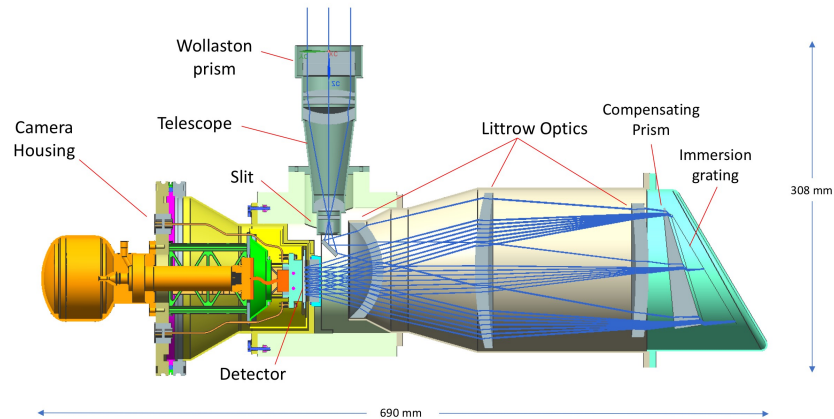


Figure 13. Simultaneous dual-polarization sensing can be implemented using the architecture illustrated here. There are two optical elements that are added to the nominal system: 1) the Wollaston Prism to angularly differentiate the polarization states at the input to the telescope, and 2) the custom polarization rotation element. The two orthogonal input polarization states are spatially encoded at the slit, but then rotated to be identical internal to the spectrometer instrument itself. In this way, the grating: 1) is used at the lowest diffraction order, 2) works at the highest grating efficiency, and 3) perfectly matches the grating efficiencies of both polarizations

4. SUMMARY AND CONCLUSION

We have presented a preliminary optomechanical design for CARBO, an innovative modular, high-sensitivity remote sensing instrument designed to deliver weekly global maps of CO₂, CH₄, CO and SIF from low Earth orbit. CARBO fills a critical gap in the Earth Science satellite program and advances key technologies – immersion gratings, detector

technology, dual polarization sensing, and modular design – to enable high-performance, cost-effective solutions for a carbon-climate observing system. Additionally, its compact, low-mass design opens up options for deployment on platforms ranging from smallsats to the International Space Station. Work continues to develop ground-based and airborne versions of CARBO to fully demonstrate these technologies and validate measurements from the current generation of greenhouse gas satellite sensors.

ACKNOWLEDGEMENTS

This research was carried out at the Jet Propulsion Laboratory, California Institute of Technology, under contract with the National Aeronautics and Space Administration. © 2016. All rights reserved.

REFERENCES

- [1] Schimel, D. et al., Observing the Carbon-Climate System, (2016), <https://arxiv.org/abs/1604.02106>
- [2] Crisp, David, et al., "The orbiting carbon observatory (OCO) mission", *Advances in Space Research* 34.4: 700-709 (2004)
- [3] Bovensmann, H., Burrows, J. P., Buchwitz, M., Frerick, J., Noël, S., Rozanov, V. V., Chance, K. V., Goede, and A. P. H., "SCIAMACHY: Mission Objectives and Measurement Modes", *Journal of the Atmospheric Sciences*. **56** (2): 127–150 (1999). <https://doi.org/10.1175/1520-0469>.
- [4] Butz, A., et al. "TROPOMI aboard Sentinel-5 Precursor: Prospective performance of CH₄ retrievals for aerosol and cirrus loaded atmospheres", *Remote Sensing of Environment* 120: 267-276 (2012).
- [5] Veefkind, J.P., Aben, I., McMullan, K., Förster, H., De Vries, J., Otter, G., Claas, J., Eskes, H.J., De Haan, J.F., Kleipool, Q. and Van Weele, M., "TROPOMI on the ESA Sentinel-5 Precursor: A GMES mission for global observations of the atmospheric composition for climate, air quality and ozone layer applications", *Remote Sensing of Environment*, 120, pp.70-83. (2012)
- [6] Buchwitz, M., Reuter, M., Bovensmann, H., Pillai, D., Heymann, J., Schneising, O., Rozanov, V., Krings, T., Burrows, J. P., Boesch, H., Gerbig, C., Meijer, Y., and Löscher, A., "Carbon Monitoring Satellite (CarbonSat): assessment of atmospheric CO₂ and CH₄ retrieval errors by error parameterization", *Atmos. Meas. Tech.*, 6, 3477-3500, doi:10.5194/amt-6-3477-2013 (2013)
- [7] Miller, C.E., et al., "Capturing Complete Spatial Context in Satellite Observations of Greenhouse Gases", *Proc. SPIE* 9976 (2016). <https://doi.org/10.1117/12.2238766>.
- [8] Frankenberg, C., Platt, U. and Wagner, T., "Iterative maximum a posteriori (IMAP)-DOAS for retrieval of strongly absorbing trace gases: Model studies for CH₄ and CO₂ retrieval from near infrared spectra of SCIAMACHY onboard ENVISAT", *Atmospheric Chemistry and Physics* 5.1: 9-22 (2005a).
- [9] Frankenberg, C., Platt, U., and Wagner, T., "Retrieval of CO from SCIAMACHY onboard ENVISAT: detection of strongly polluted areas and seasonal patterns in global CO abundances", *Atmospheric Chemistry and Physics* 5.6: 1639-1644 (2005).
- [10] Jaffe, D., "Development of Immersion Gratings to Enable a Compact Architecture for High Spectral and Spatial Resolution Imaging", NASA Grant NNX12AC31G. Final Report (2015).
- [11] Rayner, J., Bond, T., Bonnet, M., Jaffe, D., Muller, G., and Tokunaga, A., "iSHELL: a 1-5 micron cross-dispersed R=70,000 immersion grating spectrograph for IRTF", *Proc. SPIE* 8446 (2012). <https://doi.org/10.1117/12.925511>.
- [12] Park, Chan, et al., "Design and early performance of IGRINS (immersion grating infrared spectrometer)", *Proc. SPIE* 9147, (2014).
- [13] Jaffe, D., Barnes, S., Brooks, C., Lee, H., Mace, G., Pak, S., Park, B.-G., and Park, C., "GMTNIRS: progress toward the Gian Magellan Telescope Near-Infrared Spectrograph", *Proc. SPIE* 9908 (2016). <https://doi.org/10.1117/12.2232994>.
- [14] Marsh, Jasmina P., Ershov, O. and Jaffe, D., "Silicon grisms and immersion gratings produced by anisotropic etching: testing and analysis", *Proc. SPIE* 4850 (2003). <https://doi.org/10.1117/12.461759>.
- [15] Gully-Santiago, Michael A., Jaffe, Daniel T., Brooks, Cynthia B., Wilson, Daniel W., and Muller, Richard, E., "High performance Si immersion gratings patterned with electron beam lithography", *Proc. SPIE* 9151, (2014).